PAGEOPH, Vol. 133, No. 4 (1990)

0033–4553/90/040587–31$1.50 + 0.20/0
© 1990 Birkhäuser Verlag, Basel

# Two-layer Rotating Hydraulics: Strangulation, Remote and Virtual Controls[1]

LARRY PRATT[2] and LARRY ARMI[3]

*Abstract*—The hydraulics of two-layer, rotating channel flow is examined in the limit where the channel width is large compared to the internal Rossby radius of deformation, but small compared to the external deformation radius. In this limit the baroclinic flow is contained in boundary layers along each side wall, while the barotropic flow is distributed over the width of the channel. Width variations along the channel cause the strength of the barotropic flow to vary and the barotropic variations influence the baroclinic boundary layers in two independent ways. The dual nature of this forcing gives rise to a new type of critical condition which we refer to as a 'remote' control. 'Virtual' and 'narrows' controls also arise. Steady solutions can be obtained by solving a pair of simple quadratic equations and examples are given showing various combinations of controls.

**Key words:** Hydraulics, rotating hydraulics, remote control, virtual control, Fram strait, strangulation.

## *1. Introduction*

Recent field experiments in Gibraltar and other sea straits have kindled a renaissance in two-layer hydraulics (e.g., DALZIEL, 1988, 1990a,b; ARMI and FARMER, 1986, 1987, 1988; FARMER and ARMI, 1986). Although most studies concentrate on nonrotating flow, a few attempt to include rotation (WHITEHEAD *et al.*, 1974; HOGG, 1983; DALZIEL, 1988, 1990a). As the sophistication of models grows, it becomes more difficult for the nonspecialist to understand the complicated flow regimes with their multiple control points. Whereas analytic descriptions of key physical processes can be made in classical, single-layer systems, more reliance on numerical solutions is made in the multi-layer, rotational systems. These technical difficulties make it harder to illustrate the general behavior of steady solutions, particularly the along-channel structure.

---

[1] Woods Hole Oceanographic Institution Contribution No. 7252.

[2] Physical Oceanography Department, Woods Hole Oceanographic Institution, Woods Hole, MA 02543, U.S.A.

[3] Scripps Institution of Oceanography, La Jolla, CA 92093, U.S.A.

In this paper we examine the hydraulics of a system containing both multiple density layers *and* rotation in an asymptotic limit allowing simple mathematical descriptions of physical processes. In particular, we consider two-layer flow through a contraction in a rotating channel of width much smaller than the external Rossby radius (rigid lid), but much greater than the internal Rossby radius. Although there are many sea straits where such a model might be applicable (the Drake Passage, Florida Straits, Fram Strait, Bering Strait, and others) no comparisons with observations will be made. The primary purpose is to present a calculation which will provide intuition into the forcing mechanisms, critical controls, and depth and velocity structures characteristic of hydraulically-driven, two-layer flow with rotation and to point out some new dynamical properties. In the process we identify some novel features, namely a new type of forcing mechanism, a new type of critical control, and a rich variety of steady solutions.

A general formulation of the two-layer, rotating, rigid-lid problem for flow over a sill and/or through a contraction has been made by DALZIEL (1988, 1990a). DALZIEL performs the calculation using a formalism introduced by GILL (1977), which requires specification of the flow at any given cross-section in terms of a single dependent variable. The algebra involved is formidable and DALZIEL later simplifies the calculation by considering two special cases, the first having equal potential vorticities and equal and opposite flow rates in each layer (also considered by WHITEHEAD *et al.*, 1974 for zero potential vorticity) and the second having zero potential vorticity in each layer. The steady solutions for flow through a contraction and/or over an obstacle become analogous to those of nonrotating two-layer flows provided that the interface does not separate from either of the channel side walls. In particular, the influence of sills (as opposed to width contractions) on the flow rate, the placement of control sections, and the conditions for maximal exchange flow are all similar to the nonrotating analog. With separation, significant departures from nonrotating theory and even breakdown of the underlying approximations occur which are not yet completely understood. HOGG (1983) discusses some of these ideas in connection with a study of the deep flow in the Vema Channel. Similar difficulties exist in one-layer flows with rotation. In the present treatment, as in DALZIEL (1988, 1990a), we will concentrate on the nonseparated case.

We believe that the special cases considered by DALZIEL, though very instructive, eliminate some of the features which distinguish two-layer rotating flow from single-layer or nonrotational two-layer flow. These features stem from the peculiar forcing of the baroclinic portion of the flow, which can be described by reference to the strait shown in Figure 1. If the external Rossby radius of deformation is much greater than the width of the strait, the free surface of the flow is nearly horizontal. In addition, if the internal Rossby deformation radius is much smaller than the width, the slope of the interface between upper and lower layers can be significant. As will be shown, the interface can become banked against the side walls and the baroclinic part of the flow confined to boundary layers, as shown by the dashed lines

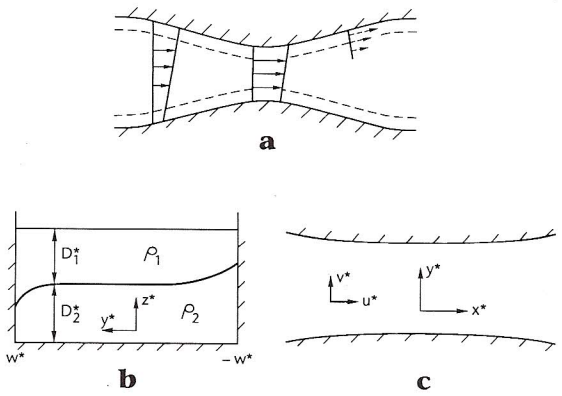


Figure 1
(a) Contracting channel with profiles of barotropic velocity (solid arrows), baroclinic velocity (dashed arrows) and the baroclinic boundary currents (dashed lines). (b) and (c) Definition sketches showing cross-sections and plan view of constant depth channel.

and arrows in Figure 1a. The barotropic part of the flow, on the other hand remains distributed across the width as shown by the solid arrows in Figure 1a.

If the barotropic and baroclinic velocities are of comparable magnitude, the total transport will be due almost entirely to the barotropic velocity since the baroclinic velocity is zero outside the thin boundary layers. As one moves along the strait and the width varies, the mean barotropic velocity varies in inverse proportion to conserve transport. Along-strait variations in the barotropic velocity can be computed from this simple statement of mass conservation.

The baroclinic boundary currents, however, are forced through more subtle mechanisms. To describe these it must be kept in mind that the changes in the barotropic velocity near a side wall force changes in the corresponding baroclinic velocity and interface height in order that energy (or Bernoulli head) be conserved. There are two ways that the side wall barotropic velocity can change; the first is associated with variations in the mean required to conserve mass, as described above. The second mechanism is more subtle and occurs when the barotropic velocity contains shear. As the strait width changes the baroclinic boundary layers are displaced laterally across this shear and experience a changing barotropic velocity.

In summary, the forcing of the baroclinic part of the flow occurs indirectly by side wall contractions through the barotropic flow and has a dual structure. We will refer to the cumulative effect of this forcing as the 'strangulation' and show that it can be more complicated than what the channel geometry alone might lead one to believe. In simpler systems, the channel width itself is commonly thought of as the 'strangulation': the narrowest section being the one where hydraulic control occurs. Here the narrowest section need not be the one where strangulation of the baroclinic part of the flow is maximum. In such cases the control section is not the

narrowest and we refer to it as a 'remote' control. This new control should not be confused with the 'virtual' control which also occurs away from the narrowest section but can arise in nonrotating applications.

Ironically the mathematical problem for the along-channel structure of the baroclinic flow is simpler in many ways than that arising in more basic applications. For example, the elevation of the interface at each channel wall can be determined at a given section by solving a simple quadratic equation, making the mathematical treatment simpler even than that of classical, single-layer hydraulics (which involves solving a cubic). This simplification allows the along-channel structure of the flow to be described easily; no numerical solutions are necessary. There is, however, one important concept, namely that of maximal baroclinic flow, which is rendered inapplicable by the asymptotic approximation. To lowest order, the steady solutions will depend only on the mass transport due to the barotropic velocity and therefore it will be impossible to identify solutions having maximal baroclinic exchange. Although such an identification could be made by going to the next order of approximation, we instead refer the reader to DALZIEL (1988, 1990a).

The following two sections develop the equations for hydraulically-driven, two-layer flow in a rotating channel. Rather than simply beginning with the equations used by DALZIEL, based on a rigid lid, we begin with a free surface and deduce the conditions under which it can be treated as rigid. Section 4 discusses the limit of large (channel width/internal deformation radius) in which case the baroclinic portion of the flow is contained in boundary layers along each side wall, while the barotropic flow is distributed across the channel. Section 4 also discusses the dual nature of the forcing mechanism for the baroclinic flow, while Section 5 identifies conditions for criticality and various types of hydraulic controls. The latter include the 'remote' control in addition to the more familiar 'narrows' and 'virtual' controls. Finally, Sections 6 and 7 give examples of various steady solutions.

## 2. *The Dimensional Equations for 2-layer Rotating Channel Flow*

Figure 1b shows our two-layer, rotating channel model in cross-section. The upper and lower layer thickness are denoted $D_1^*$ and $D_2^*$, the densities $\rho_1$ and $\rho_2$, and the channel walls lie at $y^* = \pm w^*(x^*)$. We will refer to the walls at $w^*$ and $-w^*$ as the left and right wall, as seen by an observer facing the positive $x$-direction. We assume the channel width to be gradually varying, meaning that the length scale over which $w^*$ varies is large compared to $w^*$ itself. Assuming that this geometry forces gradual along-channel variations in the steady flow, a simple scale argument suggests that $u \gg v$ and that $u_y \gg v_x$. Under this condition the along-axis velocity $u^*$ is in approximate geostrophic balance (GILL, 1977) and

the shallow water momentum equations read

$$u_1^* u_{1,x^*}^* + v_1^* u_{1,y^*}^* - f v_1^* = -g(D_1^* + D_2^*)_{x^*} \tag{2.1a}$$

$$f u_1^* = -g(D_1^* + D_2^*)_{y^*} \tag{2.1b}$$

$$u_2^* u_{2,x^*}^* + v_2^* u_{2,y^*}^* - f v_2^* = -g[(\rho_1/\rho_2)D_1^* + D_2^*]_{x^*} \tag{2.1c}$$

$$f u_2^* = -g[(\rho_1/\rho_2)D_1^* + D_2^*]_{y^*} \tag{2.1d}$$

where $f$ is the (constant) Coriolis parameter.

We further assume that the potential vorticity of the (semigeostrophic) flow is uniform within each layer:

$$(f - u_{1,y^*}^*)/D_1^* = f/D_{10} \tag{2.2a}$$

$$(f - u_{2,y^*}^*)/D_2^* = f/D_{20}. \tag{2.2b}$$

The constants $D_{10}$ and $D_{20}$ denote the 'potential thicknesses,' the thicknesses at which relative vorticity ($\cong -u_{n,y^*}^*$ in the semigeostrophic approximation) vanishes within a given layer.

It is also advantageous here to record the upper and lower layer Bernoulli laws

$$g(D_1^* + D_2^*) + \tfrac{1}{2}u_1^{*2} = B_1^*(\psi_1^*) \tag{2.3a}$$

$$(g\rho_1/\rho_2)D_1^* + gD_2^* + \tfrac{1}{2}u_2^{*2} = B_2^*(\psi_2^*) \tag{2.3b}$$

obtained by integrating (2.1) along upper and lower streamlines $\psi_1^* = \text{constant}$ and $\psi_2^* = \text{constant}$, where $\psi_n^*$ denotes the transport stream function in the $n$-th layer. If upper and lower streamlines coincide, as at a wall, (2.3b) can be subtracted from (2.3a) to give the baroclinic Bernoulli law

$$g' D_1^* + \tfrac{1}{2}(u_1^{*2} - u_2^{*2}) = B_1^*(\psi_1^*) - B_2^*(\psi_2^*) \tag{2.4}$$

where $g' = g(\rho_2 - \rho_1)/\rho_2$.

Following earlier semigeostrophic calculations we attempt to solve for the cross-stream structure of the flow first, then evaluate the along-channel dependence. Single equations for the $y^*$-structure of the layer thickness can be obtained by eliminating the velocity between (2.1b) and (2.2a) and between (2.1d) and (2.2b). The results are

$$(D_1^* + D_2^*)_{y^*y^*} - (f^2/gD_{10})D_1^* = -f^2/g \tag{2.5a}$$

$$[(\rho_1/\rho_2)D_1^* + D_2^*]_{y^*y^*} - (f^2/gD_{20})D_2^* = -f^2/g. \tag{2.5b}$$

Solving for $D_1^*$ and $D_2^*$ gives

$$D_1^* = D_{10} + \frac{A_I \cosh(\gamma_I y^*)}{\cosh(\gamma_I w^*)} + \frac{B_I \sinh(\gamma_I y^*)}{\sinh(\gamma_I w^*)} + \frac{A_E \cosh(\gamma_E y^*)}{\cosh(\gamma_E w^*)} + \frac{B_E \sinh(\gamma_E y^*)}{\sinh(\gamma_E w^*)} \tag{2.6a}$$

$$D_2^* = D_{20} - (1 - f^2/gD_{10}\gamma_I^2)\left[\frac{A_I \cosh(\gamma_I y^*)}{\cosh(\gamma_I y^*)} + \frac{B_I \sinh(\gamma_I y^*)}{\sinh(\gamma_I y^*)}\right] - (1 - f^2/gD_{10}\gamma_E^2)\left[\frac{A_E \cosh(\gamma_E y^*)}{\cosh(\gamma_E w^*)} + \frac{B_E \sinh(\gamma_E y^*)}{\sinh(\gamma_E w^*)}\right] \tag{2.6b}$$

where the $A$'s and $B$'s are functions of $x^*$ only. We have assumed that $D_1^*$ and $D_2^*$ remain finite across the entire channel width.

The along-channel velocities are obtained through substitution of the $D_1^*$ and $D_2^*$ into the geostrophic relations (2.1b,d):

$$u_1^* = \frac{-f}{\gamma_I D_{10}}\left[\frac{A_I \sinh(\gamma_I y^*)}{\cosh(\gamma_I w^*)} + \frac{B_I \cosh(\gamma_I y^*)}{\sinh(\gamma_I w^*)}\right] \frac{-f}{\gamma_E D_{10}}\left[\frac{A_E \sinh(\gamma_E y^*)}{\cosh(\gamma_E w^*)} + \frac{B_E \cosh(\gamma_E y^*)}{\sinh(\gamma_E w^*)}\right] \tag{2.7a}$$

$$u_2^* = \frac{g\gamma_I}{f}\left(\frac{\Delta\rho}{\rho_2} - \frac{f^2}{gD_{10}\gamma_I^2}\right)\left[\frac{A_I \sinh(\gamma_I y^*)}{\cosh(\gamma_I w^*)} + \frac{B_I \cosh(\gamma_I y^*)}{\sinh(\gamma_I w^*)}\right] \frac{+g\gamma_E}{f}\left(\frac{\Delta\rho}{\rho_2} - \frac{f^2}{gD_{10}\gamma_E^2}\right)\left[\frac{A_E \sinh(\gamma_E y^*)}{\cosh(\gamma_E w^*)} + \frac{B_E \cosh(\gamma_E y^*)}{\sinh(\gamma_E w^*)}\right]. \tag{2.7b}$$

The constants $\gamma_I$ and $\gamma_E$ denote the roots of

$$(\gamma^2 - f^2/gD_{10})(\gamma^2 - f^2 g D_{20}) - \gamma^4 \rho_1/\rho_2 = 0.$$

For small density differences, $(\rho_2 - \rho_1)/\rho_2 = \Delta\rho/\rho_2 \ll 1$, the roots are given by

$$\gamma_I^2 = \frac{f^2}{g'}\left(\frac{1}{D_{10}} + \frac{1}{D_{20}}\right) + O(\Delta\rho/\rho_2) \tag{2.8a}$$

$$\gamma_E^2 = f^2/g(D_{10} + D_{20}) + O(\Delta\rho/\rho_2) \tag{2.8b}$$

clearly identifying $\gamma_I^{-1}$ and $\gamma_E^{-1}$ as the internal and external deformation radii. The terms in (2.7) having subscript $I(E)$ are associated with the baroclinic (barotropic) components of the velocity fields. The scales $\gamma_I^{-1}$ and $\gamma_E^{-1}$ give the distance over which these components vary; for $w^*\gamma_I \ll 1$ or $w^*\gamma_E \ll 1$ the flow has a boundary layer structure along each wall. Note from (2.8) that the widths $\gamma_I^{-1}$ and $\gamma_E^{-1}$ of these boundary layers depend on the potential thicknesses $D_{10}$ and $D_{20}$, not the local layer thickness, and are therefore independent of $x$.

## 3. The Rigid Lid Approximation

For the remainder of the paper, discussion will focus on cases in which the external deformation radius is much larger than $w^*$ and the internal radius $\gamma_I^{-1}$, a feature common to most sea straits having strong internal hydraulic processes.

Taking the limits

$$w_E^*\gamma \ll 1$$

$$\gamma_E/\gamma_I \ll 1 \quad \left(\text{or} \quad \frac{\Delta\rho}{\rho_2} \ll 1\right)$$

in (2.6) and (2.9) lead to

$$D_1^* = \frac{A_I \cosh(\gamma_I y^*)}{\cosh(\gamma_I w^*)} + \frac{B_I \sinh(\gamma_I y^*)}{\sinh(\gamma_I w^*)} + \frac{D_{10} D^*}{D_{10} + D_{20}} \tag{3.1a}$$

$$D_2^* = -\left[\frac{A_I \cosh(\gamma_I y^*)}{\cosh(\gamma_I w^*)} + \frac{B_I \sinh(\gamma_I y^*)}{\sinh(\gamma_I w^*)}\right] + \frac{D_{20} D^*}{D_{10} + D_{20}} \tag{3.1b}$$

$$u_1^* = \frac{-f}{D_{10}\gamma_I}\left[\frac{A_I \sinh(\gamma_I y^*)}{\cosh(\gamma_I w^*)} + \frac{B_I \cosh(\gamma_I y^*)}{\sinh(\gamma_I w^*)}\right] + f\left(1 - \frac{D^*}{D_{10} + D_{20}}\right) y^* + U^* \tag{3.1c}$$

$$u_2^* = \frac{f}{D_{20}\gamma_I}\left[\frac{A_I \sinh(\gamma_I y^*)}{\cosh(\gamma_I w^*)} + \frac{B_I \cosh(\gamma_I y^*)}{\sinh(\gamma_I w^*)}\right] + f\left(1 - \frac{D^*}{D_{10} + D_{20}}\right) y^* + U^*. \tag{3.1d}$$

We have changed the definitions of the $x$-dependent coefficients (formerly $A_E$ and $B_E$) associated with the barotropic component of the flow to provide ease in physical interpretation. For example, note that the total depth is now

$$D_1^* + D_2^* = D^*(x^*). \tag{3.2}$$

The magnitude of variation of $D^*(x^*)$ can be estimated from the external Bernoulli law (2.3), which now reads

$$gD^*\left(1 + \frac{u_1^{*2}}{2gD^*}\right) = B_1^*(\psi_1^*). \tag{3.3}$$

In most sea strait flows with significant internal hydraulic signatures the quantity $u_1^{*2}/gD_* \ll 1$. Also, we anticipate that the interesting cases of the present model will occur when the barotropic velocity (the sum of the two right-hand terms in equations 3.1c,d) is the same order ($f/\gamma_I$) as the baroclinic velocity, so that $u^{*2}/gD^* = f^2/gD\gamma_I = O(\Delta\rho/\rho_2)$. In either case (3.3) indicates that the variation of $D^*$ along streamlines is negligible. Since $D^*$ has no cross-channel variation[4] we deduce $D^* =$ constant. Thus, the 'rigid' lid approximation has been obtained

[4] $D^*$ does have a weak variation in $y$ which is necessary to geostrophically support the barotropic velocity. However, it is negligible compared to individual variations in $D_1^*$ and $D_2^*$.

through the assumptions $w^*\gamma_E \ll 1$, $\Delta\rho/\rho_2 \ll 1$, and the assumption that the barotropic velocity is at most $O(f/\gamma_I)$ (i.e., the same order as the baroclinic velocity).

Evaluating the upper layer thickness at the walls gives

$$D_1^*(-w^*, x^*) = A_I - B_I + \frac{D_{10}D^*}{D_{10} + D_{20}} \tag{3.4a}$$

$$D_1^*(w^*, x^*) = A_I + B_I + \frac{D_{20}D^*}{D_{10} + D_{20}}. \tag{3.4b}$$

Thus $A_I - B_I$ and $A_I + B_I$ represent the departures at $y^* = -w^*$ and $y = w^*$ of $D_1^*$ from its resting value. Hence we shall introduce the notation

$$A_I + B_I = d^*(x) \tag{3.5a}$$

$$A_I - B_I = \hat{d}^*(x). \tag{3.5b}$$

The barotropic (layer-dependent) part of the velocity in (3.1c,d) consists of two terms, one constant in $y^*(U^*)$ and one linear in $y^*$. The presence of these terms accounts for the crucial differences between two-layer, rigid-lid hydraulics and one-layer flow with nonrigid upper boundaries. To describe the origin of these terms it is helpful to consider the case of *single-layer* flow with a rigid lid (the limit of small Froude number and large deformation radius to width ratio). Denoting the single-layer potential vorticity $f/D_0$ and taking the actual depth $D^*$ as constant, the expression for single-layer potential vorticity gives

$$u^*_{y^*} = f(1 - D^*/D_0) \tag{3.6}$$

so that

$$u^* = f(1 - D^*/D_0)y^* + U^*.$$

The velocity $u^*$ thus consists of a term $U^*$ constant in $y^*$ and a second term linear in $y^*$, both akin to the barotropic velocity components in (3.1c,d). The linear term arises when the actual thickness $D^*$ and potential thickness $D_0$ are unequal, in which case the vortex stretching effect gives rise to a uniform shear. [In the opposite case of deformation radius $\ll$ channel width, the interior depth *adjusts* to the value $D_0$. The relative vorticity therefore vanishes in the interior, becoming confined to side wall boundary layers (GILL, 1977).]

In our two-layer model, a relation similar to (3.6) can be derived by combining the expressions (2.2a) and (2.2b) for potential vorticity in the upper and lower layers. After some rearrangement the result can be written

$$\frac{\partial}{\partial y}(D_{10}u_1^* + D_{20}u_2^*) = f[D_{10} + D_{20} - D^*]. \tag{3.7}$$

From (3.1c,d) it follows that $D_{10}u_1^* + D_{20}u_2^*$ equals the barotropic velocity ($u_b^*$, *say*)

times a factor $D_{10}+D_{20}$, and (3.7) can be rewritten

$$\partial u_b^*/\partial y^* = f[1 - D^*/(D_{10}+D_{20})]$$

or

$$u_b^* = f[1 - D^*/(D_{10}+D_{20})] + U^*.$$

If the total thickness $D^*$ and sum of potential thickness is not equal, the barotropic velocity is uniformally sheared. This shear will give rise to novel and interesting implications for critical control of our two-layer rotating flow.

Having established the cross-channel structure we now address the along-channel problem; that of relating changes in cross-section to deformations of the interface. We do so using the following dimensionless versions of the thickness and velocity profiles (3.1a–d):

$$D_1 = \frac{(d+\hat{d})\cosh(y)}{2\cosh(w)} + \frac{(d-\hat{d})\sinh(y)}{2\sinh(w)} + \Delta \tag{3.8a}$$

$$D_2 = -\left[\frac{(d+\hat{d})\cosh(y)}{2\cosh(w)} + \frac{(d-\hat{d})\sinh(y)}{2\sinh(w)}\right] + \Delta/\delta \tag{3.8b}$$

$$u_1 = -\left[\frac{(d+\hat{d})\sinh(y)}{2\cosh(w)} + \frac{(d-\hat{d})\cosh(y)}{2\sinh(w)}\right] + (1-\Delta)y + U \tag{3.9a}$$

$$u_2 = \delta\left[\frac{(d+\hat{d})\sinh(y)}{2\cosh(w)} + \frac{(d-\hat{d})\cosh(y)}{2\sinh(w)}\right] + (1-\Delta)y + U \tag{3.9b}$$

where

$$D_n = D_n^*/D_{10} \quad u_n = u_n^*\gamma_I/f \quad \Delta = D^*/(D_{10}+D_{20}) \quad \delta = D_{10}/D_{20}$$

$$(x, y) = (x^*, y^*)\gamma_I \quad w = w^*\gamma_I.$$

The dependent variables are now $d(x)$ (the downward displacement of the interface at the left wall), $\hat{d}(x)$ (the downward displacement of the interface at the right wall) and $U(x) = U^*\gamma_I/f$ (the $y$-average barotropic velocity).

With this scaling the baroclinic Bernoulli law (2.4), evaluated at each side wall, becomes

$$d + \frac{(u_1^2(x, w) - u_2^2(x, w))}{2(1+\delta)} = B_1(o) - B_2(o) - \Delta \tag{3.10a}$$

$$\hat{d} + \frac{(u_1^2(x, -w) - u_2^2(x, -w))}{2(1+\delta)} = B_1(-Q_1) - B_2(-Q_2) - \Delta \tag{3.10b}$$

where $B_n = B_n^*/g'D_{10}$. The Bernoulli functions have been evaluated at $y = w$ and $y = -w$ where the values of the streamfunction have been chosen as 0 and $Q_1$ (0 and $Q_2$) for layer 1 (layer 2).

If (3.9) is used to evaluate the wall values of $u_1$ and $u_2$, (3.10a,b) provide two equations for the three unknowns $d(x)$, $\hat{d}(x)$ and $\hat{U}(x)$. To close the system, we demand that the total mass flux:

$$Q^* = \rho_1 \int_{-w^*}^{w^*} u_1^* D_1^* \, dy^* + \rho_2 \int_{-w^*}^{w^*} u_2^* D_2^* \, dy^*$$

be conserved. If the geostrophic relations (2.1b,d) are used to substitute for $u_1^*$ and $u_2^*$ and the integrals are evaluated, the dimensionless result is

$$Q = \frac{Q^* \gamma_I^2}{2\rho_2 f D} = Uw + \frac{\delta \Delta(\hat{d}^2 - d^2)}{4}. \tag{3.11}$$

The term $Uw$ clearly accounts for the barotropic transport, whereas the second right-hand term accounts for the baroclinic transport.

The expressions for mass and energy conservation derived in this section are essentially the same as those obtained by DALZIEL (1988) using a channel with a rigid lid (supporting a pressure distribution). Our results have been obtained using a free upper boundary in the limit of small channel width to external deformation radius ($w^* \gamma_E \ll 1$), small density difference ($\Delta\rho/\rho_2 \ll 1$), and small external Froude number ($u_1^{*2}/gD \ll 1$).

The foregoing discussion assumes that the interface remains attached to both side walls. It is possible for the interface to outcrop at the free surface ($D_1 \to 0$) or to intersect the bottom ($D_2 \to 0$). From (3.8a,b) these conditions arise when

$$\begin{aligned} &d < -\Delta \quad \text{(separation of upper layer from } y = w) \\ &\hat{d} < -\Delta \quad \text{(separation of upper layer from } y = -w) \\ &d > \Delta/\delta \quad \text{(separation of lower layer from } y = w) \\ &\hat{d} > \Delta/\delta \quad \text{(separation of lower layer from } y = -w) \end{aligned} \tag{3.12}$$

### 4. *The Dual Nature of the Strangulation Mechanism*

As the reader will see shortly, there is a wide variety of qualitatively different flows within the parameter space of the steady solutions. To simplify matters further and enhance our ability to provide physical interpretation, we make one further approximation, namely that of large width to internal deformation radius $w = w^* \gamma_I \gg 1$. In this limit, the expressions for the velocities at $y = w$ simplify to

$$u_1(x, w) = -d + (1 - \Delta)w + U \tag{4.1a}$$

$$u_2(x, w) = \delta d + (1 - \Delta)w + U \tag{4.1b}$$

and substitution of these into (3.10a) gives

$$d - \tfrac{1}{2} d[(\delta - 1)d + 2(1 - \Delta)w + 2U] = B_1(w) - B_2(w) - \Delta. \tag{4.2}$$

In addition, the mass balance (3.11) becomes dominated by the barotropic component as $w \to \infty$. The physical meaning of this is quite simple: since the barotropic and baroclinic velocities balance, as per previous assumption, the barotropic transport (being distributed over the entire width) greatly exceeds the baroclinic transport (which is confined to boundary layers along the side walls). Thus the mass balance is simply

$$Q = wU. \tag{4.3}$$

Substitution of $Q/w$ for $U$ in (4.2) gives

$$d^2(x) + bd(x) + c = 0 \tag{4.4}$$

where

$$b = 2[(1 - \Delta)w + (Q/w) - 1]/(\delta - 1) \tag{4.5}$$

$$c = 2[B_1(o) - B_2(o) - \Delta]/(\delta - 1). \tag{4.6}$$

The solutions thus depend upon two parameters. The second, $c$, is constant since $B_1(o)$ and $B_2(o)$ are equal to their upstream values. The first, $b$, which we will refer to as a strangulation parameter varies with the channel width and contains the side wall forcing. This forcing has a dual structure, as explained by consideration of a flow entering a constriction ($\partial w/\partial x < 0$). As the channel narrows the *average* barotropic velocity $U$ becomes larger and the side wall layers feel an acceleration due to this component of the velocity. At the same time, the side wall layers are moved to lower values of $|y|$ where the velocity due to barotropic shear, $(1 - \Delta)y$, is lower in magnitude. The latter competes with the former if $(1 - \Delta) > 0$ and their influence cancels when the strangulation parameter reaches an extreme value:

$$\frac{db}{dx} = [1 - \Delta - Q/w^2]\partial w/\partial x = 0. \tag{4.7}$$

This occurs at the narrowest cross-section ($\partial w/\partial x) = 0$ but also occurs where

$$[1 - \Delta - Q/w^2] = o,$$

or

$$w = [Q/(1 - \Delta)]^{1/2}. \tag{4.8}$$

In summary, the along-channel structure of the forcing may be more complicated than the channel geometry alone might indicate. A channel with a single width contraction (Figure 2a) containing a flow with finite barotropic shear ($\Delta \neq 1$) will contain two choke points (i.e., points of maximum strangulation) if (4.8) is satisfied at some $w$ other than the minimum $w$. In this case, the forcing of the flow is similar to that caused by a channel with 2 contractions acting on a flow with no barotropic shear, as shown in Figure 2b.

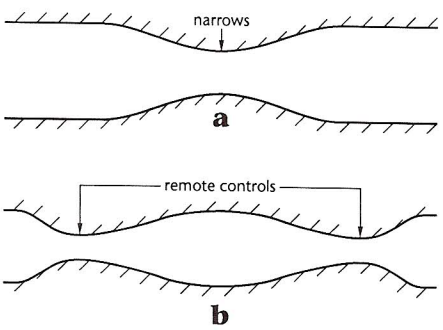


Figure 2
(a) Actual channel. (b) 'Equivalent' channel width for flow with no barotropic shear.

We note that the expressions for $b$ and $c$ in (4.5) and (4.6) become singular when $\delta = 1$, corresponding to equal potential vorticities in each layer. In Section 6 we show that the interface is separated from one of the side walls in this case and discussion will therefore be restricted to the case $\delta \neq 1$.

Equation (4.4) determines the interface displacement along the wall at $y = w$. The corresponding relation at $y = -w$ is

$$\hat{d}^2 + \hat{b}\hat{d} + \hat{c} = 0 \tag{4.9}$$

where

$$\hat{b} = 2[(1-\Delta)w - (Q/w) - 1]/(\delta - 1) \tag{4.10}$$

$$\hat{c} = 2[B_1(Q_1) - B_2(Q_2) - \Delta]/(\delta - 1) \tag{4.11}$$

and from (4.7) strangulation of this portion of the flow vanishes where $w_x = 0$ or where

$$w = [-Q/(1-\Delta)]^{1/2}. \tag{4.12}$$

The only source of asymmetry between left and right walls is the barotropic transport $Q$; for example, a positive $Q$ in the absence of a baroclinic flow will retard the left wall Kelvin wave speed, but will augment the right wall Kelvin wave speed. Note that the coefficients in (4.9) are identical to those in (4.4) if $Q$ is replaced by $-Q$. Although the structure of the baroclinic boundary layers is determined independently of each other (equations (4.4) and (4.9) contain no cross terms), the flow within a given boundary layer *does* respond to changes in position of the opposite wall. This communication is carried by the barotropic flow which responds to changes in either side wall. In contrast, single-layer rotating-channel flows with a boundary layer structure have quiescent interiors and experience no wall-to-wall communication.

Virtually the whole range of effects discussed in the remainder of the paper are contained in equations (4.4)–(4.6).

## 5. Critical Flow and Hydraulic Control

The most important steady flow solutions will be ones which pass through one or more critical sections, i.e., sections where the linear phase speed $\lambda_+^*$ or $\lambda_-^*$ of one of the side-wall Kelvin waves vanishes. For a discussion of critical flow, its relation to hydraulic control, and the conditions under which critically-controlled states are preferred, the reader is referred to BAINES (1984) or PRATT and ARMI (1988) and references contained therein. In Appendix A we calculate the Kelvin wave phase speeds, with dimensional result

$$\lambda_\pm^* = \frac{u_1^*(\pm w^*, x)D_{20} + u_2^*(\pm w^*, x)D_{10}}{D_{10}+D_{20}} \mp \frac{(g'D_{10}D_{20})^{1/2}}{(D_{10}+D_{20})^{1/2}} \tag{5.1}$$

where $u_1^*(\pm w, x)$ and $u_2^*(\pm w, x)$ are the wall velocities of the basic flow upon which the linear wave propagates. Equation (5.1) is valid in the wide-channel limit $w^*\gamma_I \to \infty$, in which case the Kelvin wave trapped at the left wall does not feel the right wall, and *vice-versa*. From the form of the linear wave speed we define $y = \pm w^*$ Froude numbers by

$$F_\pm = \frac{u_1^*(\pm w^*, x)D_{20} + u_2^*(\pm w^*, x)D_{10}}{\mp[g'D_{10}D_{20}(D_{10}+D_{20})]^{1/2}} \tag{5.2}$$

when $F_+ = 1$ ($F_- = 1$) the flow is critical with respect to the $y^* = w$ ($y^* = -w^*$) Kelvin wave.

In dimensionless terms the Kelvin wave speeds are

$$\lambda_\pm = \lambda_\pm^*\gamma_I/f = \frac{u_1(\pm w, x) + \delta u_2(\pm w, x)}{1+\delta} \mp 1.$$

Using (3.9), (4.5) and (4.10) this expression simplifies to

$$\begin{aligned}\lambda_+ &= (\delta-1)d + (1-\Delta)w + U - 1 \\ &= (\delta-1)d + \tfrac{1}{2}(\delta-1)b\end{aligned} \tag{5.3}$$

for the left wall Kelvin waves, and

$$\begin{aligned}\lambda_- &= (1-\delta)\hat{d} - (1-\Delta)w + U + 1 \\ &= -(\delta-1)\hat{d} - \tfrac{1}{2}(\delta-1)\hat{b}\end{aligned} \tag{5.4}$$

for the right wall Kelvin wave.

Using the terms subcritical, critical, and supercritical to denote wave speeds $<0$, $=0$, and $>0$ we have

$$\lambda_+ = (\delta-1)(d+b/2) \quad \begin{cases} <0 \text{ (subcritical)} \\ =0 \text{ (critical)} \\ >0 \text{ (supercritical)} \end{cases} \tag{5.5a}$$

with respect to the left wall Kelvin wave, and

$$\lambda_- = -(\delta - 1)(\hat{d} + \hat{b}/2) \quad \begin{matrix} < 0 \text{ (subcritical)} \\ = 0 \text{ (critical)} \\ > 0 \text{ (supercritical)} \end{matrix} \tag{5.5b}$$

with respect to the right wall Kelvin wave.

The locations of critical sections can be ascertained through differentiation of (4.5) and (4.9) with respect to $x$, resulting in

$$d_x = -\tfrac{1}{2} d b_w w_x / (d + b/2) \tag{5.6a}$$

$$\hat{d}_x = -\tfrac{1}{2} \hat{d} \hat{b}_w w_x / (\hat{d} + \hat{b}/2). \tag{5.6b}$$

When the denominator in (5.6a or b) vanishes the flow is critical and the numerator must also vanish so that the $d_x$ or $\hat{d}_x$ remain bounded. The latter occurs under one of several conditions: First the strangulation can reach an extreme value ($db/dx = b_w w_x = 0$). This condition can occur at a narrows ($w_x = 0$), in which case we refer to the critical flow section as a 'narrows' control. It is also possible that $b_w = 0$, a condition which can occur away from the narrowest section. This new type of control condition is made possible by the dual nature of the strangulation and will be referred to as a 'remote' control. The value of $w$ at such a control is given by

$$w = [Q/(1 - \Delta)]^{1/2} \tag{5.7a}$$

for the left boundary flow, and

$$w = [-Q/(1 - \Delta)]^{1/2} \tag{5.7b}$$

for the right boundary flow.

The final condition for vanishing of the numerator in (5.6a or b) is that $d$ (or $\hat{d}$) vanishes, meaning that the baroclinic flow component (the vertical shear) disappears. This condition arises in 2-layer nonrotating hydraulics (ARMI, 1986; WOOD, 1968) and is referred to as a virtual control. It generally occurs at a section other than the narrowest.

The actual interface slope at a control section can be calculated from (5.7a or b) by applying L'Hopitals' rule. For (5.6a) we have

$$d_x = \lim_{d \to b/2} \frac{d/dx(-\tfrac{1}{2} d b_w w_x)}{d/dx(d + b/2)}.$$

Using (4.4) to express $b_x$ in terms of $d_x$, we obtain

$$(d_x)^2 = -\tfrac{1}{2}(d_x b_w w_x + d b_{ww} (w_x)^2 + d b_w w_{xx}). \tag{5.8}$$

In general, two interface slopes (corresponding to the two roots in 5.8) are possible for a given critical value of $d$. These are the slopes of two possible solution

branches (corresponding to the two roots of 4.4) crossing each other at the control section.

The inequalities in (5.5b) have been chosen with the idea that $x \to -\infty$ represents upstream. Thus 'subcritical' flow represents propagation of the $y = w$ Kelvin wave in the minus $x$-direction. There are situations where it may be more reasonable to choose $x \to \infty$ as upstream and to reverse the inequalities in (5.5b).

For flow in the $y = w$ boundary current the critical values of $d$ and $w$ are related by

$$d_c = -b(w_{c+})/2 = \pm c^{1/2} \tag{5.9a}$$

in view of (5.5a) and (4.4). Here $w_{c+}$ is the value of $w$ at which the numerator in (5.6a) vanishes. The corresponding expression for the $y = -w$ flow is

$$\hat{d}_c = -\hat{b}(w_{c-})/2 = \pm \hat{c}^{1/2} \tag{5.9b}$$

where $w_{c-}$ is now the width at which the numerator in (5.6b) vanishes.

If the definitions of $b$ and $\hat{b}$ are used in (5.9a,b) the results are

$$d_c = -[(1-\Delta)w_{c+} + Q/w_{c+} - 1]/(\delta - 1) \tag{5.10a}$$

$$\hat{d}_c = -[(1-\Delta)w_{c-} - Q/w_{c-} - 1]/(\delta - 1). \tag{5.10b}$$

If the location of a critical section ($w = w_{c+}$ or $w = w_{c-}$) is known in advance measurement of $d_c$ (or $\hat{d}_c$) along with predetermination of the constants $\Delta$ and $\delta$ gives the barotropic transport. Equations (5.10a and b) are extensions of the weir formula of open channel flow which allow transport determination by measurement of fluid depth at a critical section. (For example the transport at a control section in a single layer flow is given by $Q^* = 2w^* g^{1/2} D^{*3/2}$.) The present case is complicated by the fact that the potential thicknesses for the two layers (as contained in $\delta$ and $\Delta$) must also be determined.

The foregoing discussion was written under the assumption that the reader would be familiar with the meaning of the critical condition and its implications for hydraulic control (or upstream influence) over the steady flow. However, we will briefly discuss the idea of upstream influence in the context of the present model. Discussion will be restricted to the boundary layer flow at $y = w$. If (4.4) is evaluated at the critical section $w = w_{c+}$ and (5.9) is used, the result is

$$c = b^2(w_{c+})/4 \tag{5.11a}$$

or

$$2[B_1(o) - B_2(o) - \Delta](\delta - 1) = [(1-\Delta)w_{c+} + Q/w_{c+} - 1]^2. \tag{5.11b}$$

In a steady flow with a critical section, there is a fixed relation between the parameters $\Delta$, $\delta$, $Q_1$ and $B_1 - B_2$ (which specify the upstream flow) and the geometric parameter $w_{c+}$. The upstream flow parameters cannot be varied independently of $w_c$, as they *can* when no critical section exists, and we say that

the upstream flow is controlled (or that upstream influence exists) at the critical section.

If the control section represents a narrows control $w_{c+}$ is fixed. For a virtual control, $d_c = 0$ (no baroclinic flow) and therefore $c = 0$, or

$$B_1(o) - B_2(o) = \Delta.$$

Here upstream influence implied a relationship between $B_1(o)$, $B_2(o)$, and $\Delta$. Finally, if the control is of the remote type, $w_{c+} = [Q/(1-\Delta)^{1/2}]$ and (5.11b) becomes

$$2[B_1(o) - B_2(o) - \Delta](\delta - 1) = [2Q^{1/2}(1-\Delta)^{1/2} - 1]^2.$$

Critical control of the right boundary layer implies a similar set of constraints, the main difference being that $B_1(o) - B_2(o)$ is replaced by $B_1(Q_1) - B_2(Q_2)$.

To summarize this section, we have derived the conditions for critical flow and identified geometrical and dynamical conditions for its existence. Two distinct conditions have been found, the first being that the strangulation effect of the barotropic on the baroclinic flow reach an extreme. This can occur at a 'narrows control,' where $\partial w/\partial x = 0$, or at a 'remote control,' where $\partial b/\partial w = 0$. The second condition can occur when the baroclinic part of the flow disappears, $d = 0$, corresponding to a 'virtual' control. As we shall see, 'remote' and 'narrows' controls are dynamically similar whereas virtual controls are more unique.

## *6. Steady Solutions with 'Narrows' and 'Remote' Controls*

Steady solutions for the barotropic flow and the left and right baroclinic boundary layers can be computed independently. The former is given simply by $U(x) = Q/w(x)$. The boundary layer components are found by first calculating $b$ or $\hat{b}$ as functions of $x$. (Remember that $b$ and $\hat{b}$ are the strangulation parameters for the left and right walls.) To do so, we find $b(w)$ or $\hat{b}(w)$ from equations (4.5) or (4.10), then use the prespecified $w(x)$. Once $b$ and $\hat{b}$ are known, the interface displacements $d$ or $\hat{d}$ are computed from the energy constraints (4.4) or (4.9). The parameters needed are $\delta$, $\Delta$, $Q$, and $B_1(o) - B_2(o)$ (for the $y = w$ boundary flow) or $B_1(Q_1) - B_2(Q_2)$ (for the $y = -w$ boundary flow).

Figure 3 contains plots showing the behavior of $b(w)$ and $\hat{b}(w)$ for various values of $Q$ and $\Delta$. Figure 3a shows the case $Q > 0$ (positive mean barotropic flow) and $\Delta < 1$ (positive barotropic shear). The curve of $b(w)$, actually displayed as $(\delta - 1)b(w)$, contains an extremum while $\hat{b}(w)$ is monotonic. Thus, a remote control is possible for the left-hand boundary flow only. Virtual control is possible wherever either forcing curve intersects the $w$ axis ($b$ or $\hat{b}$ vanishes). For the parameter settings used to draw Figure 3a the only such intersection occurs in the

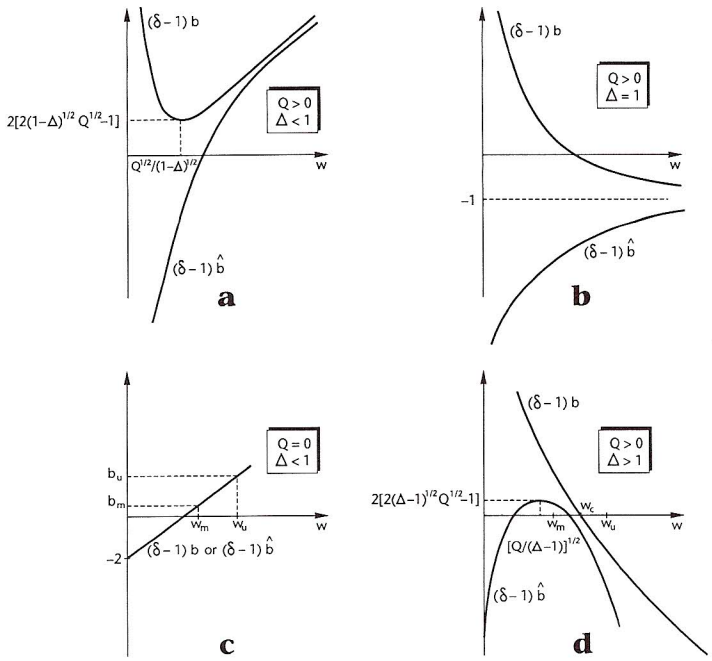


Figure 3
'Forcing' curves giving the strangulation parameters $b$ and $\hat{b}$ as functions of $w$ for various barotropic transport $Q$ and shear parameter $\Delta$. The curves are based on equations (4.5) and (4.10).

$(\delta - 1)\hat{b}$ curve. Thus a virtual control is possible for the right-hand boundary flow only. Should we have chosen $[2(1 - \Delta^{1/2})Q^{1/2} - 1] < 0$, lowering the minimum of the $(1 - \delta)b$ curve below the $w$ axis, then two virtual controls at different widths (but the same strangulation, $b$) corresponding to the two zeros of this curve would have become possibilities.

In Figure 3b the case $\Delta = 1$ (no barotropic shear) is shown for $Q > 0$. Figure 3c covers the case of no mean barotropic flow ($Q = 0$), which includes exchange flows, and is drawn for $\Delta < 1$. In both Figures 3b and 3c, one of the barotropic forcing mechanicms is absent and the forcing curves are monotonic. Intersections of the forcing curves with the $w$-axis indicate possible virtual controls. Narrows controls are also possible, but not remote controls. Should the barotropic flow vanish completely ($\Delta = 1$ and $Q = 0$) the forcing vanishes and, at the present order of approximation, the baroclinic boundary layers maintain a fixed structure.

Finally, Figure 3d covers the case of negative barotropic shear ($\Delta > 1$) and $Q > 0$. Only $\hat{b}(w)$ contains an extremum, corresponding to a possible remote control, whereas both $b(w)$ and $\hat{b}(w)$ have zeros, corresponding to possible virtual controls.

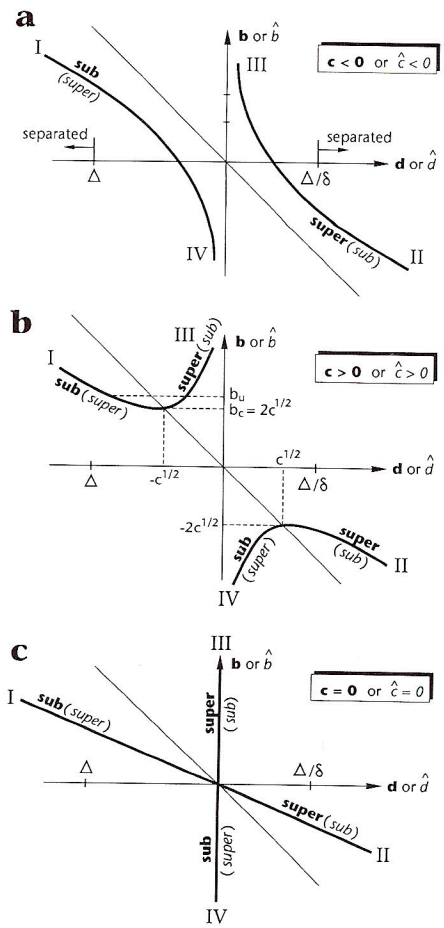


Figure 4

Solutions to equation (4.4) for various values of $c$. Solutions to (4.9) for the right-hand boundary flow can also be obtained by reading the labels written in italics. The diagonal line in each figure represents critical flow ($d = -b/2$), with supercritical values of $d$ lying above and subcritical values below.

Figure 4 contains examples of solution curves for equation (4.4) (or 4.9), relating the strangulation $b(x)$ (or $\hat{b}(x)$) to the downward interface displacement $d(x)$ (or $\hat{d}(x)$) at the left (or right) wall. The qualitative structure of the curves changes depending on whether $c$ (or $\hat{c}$) is $<o$, $>o$, or $=o$ and we have sketched an example from each case. Remember that $c$ is a measure of the energy difference between layers (see 4.6). In order to reconstruct the behavior of $d$ with changing $w$ it is necessary to use the Figure 4 curves in connection with the Figure 3 curves, and we have therefore chosen $b$ as the ordinate in each Figure. The Figure 4 curves can also be used to determine $\hat{d}$ in terms of $\hat{b}$ by using the axis and curve labels

indicated in italics. Figure 4a is drawn for the case $c < 0$ and shows two distinct, monotonic solution curves. The diagonal line $b = -2d$ corresponds to critical flow and divides the $(d, b)$ plane into supercritical and subcritical regions. For $\delta > 1$, solutions above the diagonal are supercritical and those below subcritical, as shown by equation (5.5). Thus the upper right-hand curve corresponds to supercritical solutions and the lower left-hand curve to subcritical solutions; critical flow is not possible.

We have also indicated the values $d < -\Delta$ and $d > \Delta/\delta$, corresponding to separation of the upper and lower layer. In these ranges the depth and velocity profiles must be reformulated and the solutions shown are invalid. Computation of the separated flow is beyond the scope of this paper. The right wall separation conditions are given by $\hat{d} < -\Delta$ and $\hat{d} > \Delta/\delta$.

### *6a. Two Noncontrolled Flows*

The construction of a solution will now be demonstrated by an example. Consider a channel with a single contraction at $x = 0$ having minimum width $2w_m$ and width $2w_u$ at $x = \pm\infty$ (Figure 5a), and assume that $c < 0$, $\hat{c} < o$, $\delta > 1$, $Q = 0$ and $\Delta < 1$. The curve relating $w$ to $b$ will be of the type shown in Figure 3c. If we begin at a point $x < o$ upstream of the contraction, where $w = w_u$, then $b = b_u$ as indicated in Figure 3c. Moving downstream and into the narrowest part of the contraction causes $w$ to decrease to $w_m$ and $b$ to decrease to $b_m$, also labelled in Figure 3c. Downstream of the contraction $b$ returns to its upstream value $b_u$. For our choice $c < o$, the relation between $d$ and $b$ is given in Figure 4a and we see that two solutions are possible, one subcritical and one supercritical, for the range $b_m < b < b_u$. In both cases $d$ increases as one moves from upstream into the narrowest section then returns to its upstream value as one moves further downstream. The interface profile at $y = w$ is sketched in Figure 5b for the subcritical solution; the supercritical solution is similar.

Additional information is required to choose between the supercritical and subcritical solutions in the above example. Sometimes the qualitative nature of the upstream flow is known in advance and this determines the desired solution. If the channel widens into a basin upstream, for example, $b_u$ becomes very large implying that the subcritical solution is separated from the left wall (Figure 4a shows that $d \to -\infty$), while the supercritical solution remains attached ($d \to 0$). If it is known that the flow *is* attached upstream, or if the separated solution is considered undesirable on philosophic grounds, the supercritical solution is chosen.

Determination of $d(x)$ fixes the structure of the $y = w$ boundary flow. For example, the thickness and velocity profiles near $y = w$ are given by (3.8) and (3.9) with $w \to \infty$:

$$D_1 = de^{-(w-y)} + \Delta \tag{6.1a}$$

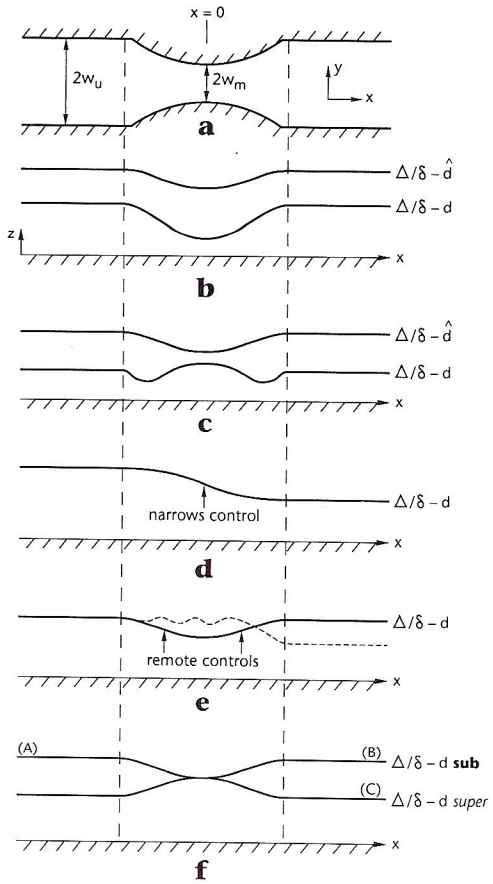


Figure 5

(a) Plan view of channel with single contraction used in all examples. Figures 5b–5d show the interface elevations $(\Delta/\delta) - d$ and $(\Delta/\delta) - \hat{d}$ at the left and right walls, $y = w$ and $y = -w$; for (b) $Q = 0, \Delta < 1, \delta > 1, c < 0, \hat{c} < 0$; (c) same as (b) but with $Q > 0$. (d) Left-wall profile for $Q > 0, \Delta < 1, \delta > 1, c < 0$ and $w_m > Q^{1/2}/(1-\Delta)^{1/2}$; (e) same as (a) but $w_m < Q^{1/2}/(1-\Delta)^{1/2}$; the dashed curve shows how the solution might be altered by an instability near the second (right-hand) remote control; (f) possible interface elevations at $y = w$ when a virtual control occurs at the section of minimum width.

$$D_2 = -de^{-(w-y)} + \Delta/\delta \tag{6.1b}$$

$$u_1 = -de^{-(w-y)} + (1-\Delta)y + U \tag{6.2a}$$

$$u_2 = \delta de^{-(w-y)} + (1-\Delta)y + U. \tag{6.2b}$$

Since the forcing curve for $b$ is identical to that for $\hat{b}$ in Figure 3c, and since the solution curve for $\hat{d}$ is contained in Figure 4a, determination of the interface at the right wall is identical to the procedure described above. Figure 5b also shows the right-wall result when the subcritical branch is selected.

For a slightly more interesting example reconsider the above parameter settings with $Q > 0$, in which case $b(w)$ is given by the upper curve in Figure 3a. This curve has a minimum at $w = Q^{1/2}/(1-\Delta)^{1/2}$. Further suppose that $w_u > Q^{1/2}/(1-\Delta)^{1/2} > w_m$, in which case one passes through the minimum in the $b(w)$ curve as $w$ decreases. Thus $b$ initially decreases as one enters the contraction, but begins to increase before the narrowest section is reached. Downstream of the narrowest section $b(w)$ decreases, then increases to its upstream value as suggested in Figure 2b. Applying this forcing to the subcritical solution curve in Figure 4a shows that the upper layer depth increases, then decreases, as one approaches the narrowest section, with similar behavior downstream. The interface elevation at the left wall (Figure 5c, lower curve) has three extrema, a consequence of the dual nature of the forcing mechanism. The behavior of $\hat{b}(w)$ for this case is determined by the lower curve in Figure 3a. Since $\hat{b}$ increases monotonically with $w$ the variation of $\hat{d}(w)$ through the narrows is qualitatively the same as in the first example. The interface elevation along the right wall is also shown in Figure 5c.

### *6b. A Flow with a Narrows Control*

We now move to several examples having $c > 0$, so that the solution curve for $d$ is given by Figure 4b. Also let $\delta > 1$, $Q > 0$ and $\Delta < 1$ so that the forcing curve for the left wall flow continues to be the upper curve in Figure 3a. First, suppose that $w_u > w_m > Q^{1/2}/(1-\Delta)^{1/2}$, so that the range in $w$ lies to the right of the minimum of the forcing curve and thus $b$ decreases monotonically with decreasing $w$ (Figure 3a). As the contraction is entered the value of $b$ decreases from its upstream value $b_u$. To find the corresponding $d$, one must choose a supercritical or subcritical branch from the appropriate curve in Figure 4b. Here, Figure 3a gives a positive $b$ and the *upper* left-hand curve in Figure 4b is therefore appropriate. We choose the subcritical branch (labeled I) of this curve for the upstream flow and the value $b_u$ has been marked on Figure 4b. As one moves downstream into the narrows ($b$ decreases) $d$ increases. If the minimum value $b_m$ is greater than the minimum (or critical) value $b_c$ for the solution curve, the maximum value of $d$ occurs at the narrowest section. If, on the other hand, $b_m = b_c$ the solution can flip from branch I to III of the Figure 4b curve, causing $d$ to continue to increase downstream of the narrowest section, as shown in Figure 5d. The $y = w$ boundary flow is thus subcritical upstream of the narrowest section and supercritical downstream, so that a narrows control exists. It is also possible to choose the supercritical branch (labeled III) upstream of the contraction, in which case attachment of the boundary flow is guaranteed for arbitrarily large upstream widths. However this selection leads to an instability, detailed below, which makes the choice undesirable.

In the present example, it is not obvious that the solution *must* flip from the subcritical to supercritical branch of the upper curve in Figure 4b. To investigate this situation more closely, consider the regularity condition (5.8) at the branch

point $b = b_c$, here a narrows control. Setting $\partial w/\partial x = 0$ gives

$$d_x^2 = -\tfrac{1}{2} d b_w w_{xx} \quad (b - b_c).$$

Now $d < o$ and $b_w > o$, as inspection of the solution and forcing curves indicate, and $w_{xx} > o$ at a contraction, thus $d_x^2$ is positive. Nonzero $d_x$ implies that the solution does in fact change branches, positive $d_x$ corresponding to a shift from subcritical to supercritical branches.

### *6c. Flow with Remote Controls*

A more intriguing variation of the last case occurs when $w_m < Q^{1/2}/(1-\Delta)^{1/2} < w_u$, so that $b$ goes through a minimum value $b_m$ before the narrowest section is reached (Figures 3a and 2b). If $b_m = b_c$ the solution curve (Figure 4b) will flip from Branch I to Branch III at the section where $w = Q^{1/2}/(1-\Delta)^{1/2}$, i.e., at a remote control. Inspection of the regularity condition (5.8) indicates that the solution does indeed change branches. Beginning upstream of the narrows, the value of $d$ increases until the narrowest section is reached, passing through critical value $d_c$ at an intermediate section. The value of $d$ then decreases again, passing through $d_c$ a second time. This solution is sketched in Figure 5e. Near the second remote control, where the transition from supercritical to subcritical occurs, the flow is unstable. PRATT (1984) has discussed this instability in connection with single-layer, nonrotating flow over two sills of identical elevation. Hydraulic theory predicts a stable (subcritical-to-supercritical) transition over the first (upstream) sill and an unstable (supercritical-to-subcritical) transition over the second (downstream) sill. Laboratory experiments indicate that the flow is subcritical and wave-like over the first obstacle and that a subcritical-to-supercritical transition occurs over the second obstacle. The latter is predicted by a theory taking weak dispersive effects into account. Should similar behaviour occur here, the dashed curve in Figure 5e gives a qualitative picture of what the interface profile would look like.

The $y = -w$ boundary flow is determined by the lower forcing curve in Figure 3a, and remote control is impossible since this curve has no extremum. Depending on the value of $\hat{c}$ the flow may experience a narrows control (as shown in Figure 5d), a virtual control or may be noncontrolled.

### *6d. 'Remote' Controls at the Narrowest Section*

From the previous examples it is clear that critical control occurs at the most strangulated section or sections (i.e., that having the smallest value of $b$). If $w_m > Q^{1/2}/(1-\Delta)^{1/2}$ the minimum $b$ occurs at the narrowest section, while $w_m < Q^{1/2}(1-\Delta)^{1/2}$ implies minimum $b$ at some other section.

A special case occurs when the minimum width is identical to the critical width for a remote control

$$w_m = Q^{1/2}/(1-\Delta)^{1/2}.$$

If the flow is critical, remote and narrows controls coincide. The regularity condition then reduces to (5.8)

$$d_x^2 = 0 \tag{6.3}$$

i.e., the interfacial slope vanishes for both the subcritical and supercritical solution branches, corresponding to the two roots of (6.3). In this case the two solution branches make grazing contact at the narrowest section, as sketched in Figure 5f. Choosing the subcritical branch (labeled A) upstream, it is possible to move onto the supercritical branch (labeled C) or the subcritical branch (labeled B) at the narrowest section, $x = o$. Repeated differentiation of (4.4) and use of L'Hopitals rule shows that

$$d_{xx}^2 = -\tfrac{1}{2} db_{ww}(w_{xx})^2$$

at $x = o$ when narrows and remote controls merge. For the parameters of the current example $d < o$ and $b_{ww} > o$, so that $d_{xx}$ takes on a separate finite value for each solution branch. Choosing the subcritical branch B downstream implies continuity of $d_{xx}$ at $x = o$. However, this solution is subcritical everywhere except at $x = o$ and is therefore, not critically-controlled. The other alternative is to choose the supercritical branch C downstream. This solution has discontinuous $d_{xx}$ at $x = o$, but has the virtue of being critically-controlled. Since critically-controlled states seem to be the preferred asymptotic solutions in adjustment experiments (e.g., BAINES, 1984), it is possible that this second combination is preferred in practice, with some local departure in long-wave theory occurring near $x = o$.

By now it will be obvious to the reader how to construct the flow in the right boundary layer and we will refrain discussion of this part of the flow here and in subsequent examples.

### *6e. The Case $\delta = 1$: Equal Potential Vorticities*

Finally, we discuss the special case $\delta = 1$ corresponding to equal potential vorticities in each layer. Although equation (5.5) appears to indicate that the flow is always critical ($\lambda_+ = 0$) for $\delta = 1$, this is not the case. A factor of $(\delta - 1)^{-1}$ appears in the definitions of $b$ and $c$, and these variables must be rescaled in order to discuss the limit $\delta \to 1$. By doing so it can be shown that the critical values of $d$ and $\hat{d}$ grow without bound as $\delta \to 1$, implying that the interface is separated from the side wall. One example is an exchange flow having equal potential vorticity in each layer (DALZIEL, 1988, 1990a). The flow separation, confirmed by DALZIEL's calculation, is beyond the scope of the present theory.

## 7. *Solutions with Virtual Controls*

At a virtual control the interface displacement ($d$ or $\hat{d}$) at the appropriate wall vanishes. Equation (4.4) or (4.9) then implies that $c = o$ or $\hat{c} = o$, and the corresponding solution curves are shown in Figure 4c. These curves intersect each other at the virtual control, also the origin ($d = b = o$ or $\hat{d} = \hat{b} = o$), raising the possibility that the solution might jump from one branch to another (branch I to branch III, say) upon crossing the origin. In Appendix B, we show that such a jump would imply a discontinuity in $d_x$ or $d_{xx}$ at the control and we therefore require that solutions on curve I-II do not jump to curve III-IV or *vice-versa*. The only exception occurs when narrows, remote, and virtual controls coincide at the narrowest section, a case discussed more fully in Appendix B. Here, we assume otherwise.

Before a meaningful example of virtually-controlled solutions can be constructed, we must discuss the stability of the solutions to weak frictional perturbations. In most geophysical applications of the present theory, bottom friction will dominate other sources such as side-wall or interfacial friction. Bottom friction tends to decrease the value of the lower layer Bernoulli function $B_2(\psi)$ in the direction of the flow and this results in an increase in the constant $c$ (or $\hat{c}$). Friction thus results in a gradual increase in $c$ (or $\hat{c}$) in the direction of the lower layer flow. This increase leads to no qualitative departures from the solutions described in previous examples; however, the virtually-controlled solution curves undergo profound changes in form when $c$ is slightly different from zero. For $c > o$ the solution curves of Figure 4c are deformed into curves resembling those of 4b. The solutions I-II and III-IV are broken so that branch I connects only with III and II only with IV. For $c < o$ the curves resemble the Figure 4a curves, so that branch I connects with IV and III with II. It should also be noted that weak friction can cause slow variations in the potential vorticity of the fluid. In the context of the present model this process can be thought of as a slow variation in $\delta$ and $\Delta$. However, these variations cause no essential changes in the topology of the forcing or solution curves and therefore amount to a weak background effect.

Now consider an example in which $\delta > 0$, $Q > o$ and $\Delta > 1$, so that the strangulation is given by the upper curve in Figure 3d, and $c = o$. For the moment, we neglect any weak frictional effects which would introduce slow variations in $c$. In order for the virtual control to occur, the forcing curve must have a zero and we therefore choose our range of $w$ to indicate the zero in the Figure 3d upper curve ($w_u > w_c > w_m$). The strangulation parameter $b$ thus is negative far upstream and downstream, but positive at the narrowest section.

Moving now to Figure 4c and beginning far upstream of the narrows ($b < o$), we choose the subcritical solution branch (the negative $b$-axis). As $w$ decreases $b$ increases and the virtual control ($b = o$) is passed before the narrowest section is reached. Downstream of the narrowest section $b$ returns to negative values, passing

through a second virtual control. This second control involves supercritical-to-subcritical flow and is subject to the instability discussed earlier in connection with remote controls. In the latter, one is forced to consider non-semigeostrophic dynamics in order to construct a stable solution. Here, weak friction tends to remove the unstable control point altogether, as described below.

Now consider the influence of weak friction on the solution described above when the velocity in the lower layer is positive at the left wall. The lower layer Bernoulli function at the left wall $B_2(o)$ decreases, and $c$ increases, with increasing $x$. Beginning upstream on branch IV in Figure 4c, we again attempt to construct a solution by observing the effect of increasing $b$. As $b$ increases, $c$ increases due to friction and branch IV is deformed into branch IV of Figure 4b. The point $b = o$ cannot now be reached because the maximum of the new curve occurs at a negative value of $b$. Furthermore, it is not possible to connect to another solution through a hydraulic jump because the upstream flow would be required to be supercritical.

In order to pass through the virtual control $c$ must clearly be $< o$ upstream of the contraction and the effect of friction must be such as to bring $c$ to zero just as $b$ vanishes. Suppose that this is the case and consider the supercritical flow downstream of the virtual control, where $b > o$. As one moves downstream from the control $c$ continues to increase, becoming positive, and branch III in Figure 4c is deformed into branch III in Figure 4b. After the narrowest section is passed $b$ decreases again until the minimum in the latter is encountered. Since the flow is supercritical it may be possible to remove this dilemma by placing a hydraulic jump in the flow. Jumps dissipate energy and alter potential vorticity in complicated ways (PRATT, 1983; NOF, 1986) so that prediction of the change in $c$ across the jump is difficult. One possibility would be for $c$ to become $< o$ downstream of the jump, allowing the solution to connect to branch I-IV in Figure 4a and thus return to negative values of $b$.

The circuit in the $(d, b)$-plane mapped out by this solution is drawn in Figure 6a. The arrows indicate the direction of increasing $x$ and the corresponding interface elevation is sketched in Figure 6b. We pose this only as a plausible solution relying on future laboratory experiments to confirm it.

If the lower layer flow is reversed along the left wall ($u_2 < o$ at $y = w$), $c$ will decrease in the positive $x$ direction. For the forcing described in the above example, $c$ must be $> o$ for large negative $x$ in order for a virtual control to occur. As one approaches the narrows from upstream, the lower layer energy at the left wall, $B_2(o)$, slowly increases causing $c$ to decrease to zero at the virtual control. Downstream $c$ becomes negative and the solution (branch III in Figure 4c) is deformed into branch III of Figure 4a. The full solution is mapped out $(d, b)$-space in Figure 6c and the corresponding interface profile is shown in Figure 6d.

In the two previous examples of virtually-controlled flow $|d|$ is small over the portions of channel upstream of and immediately downstream of the control. It follows that the interfacial shear $(u_1 - u_2)$ near the left wall is small as well, making

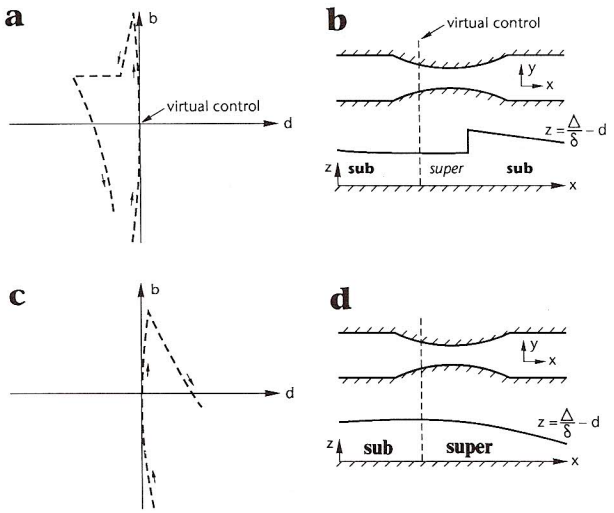


Figure 6
(a) Path in $(d, b)$-plane mapped out by a virtually-controlled solution with positive velocity at $y = w$. (b) Plan view of channel and interface elevation of $y = w$ for solution mapped out in (a). (c) and (d) correspond to a flow with reverse flow at $y = w$.

this solution analogous to the virtually-controlled solutions for unidirectional flow described by WOOD (1968) and ARMI (1986) in connection with nonrotating, two-layer flow.[5] A second class of virtually-controlled solutions, associated with I-II in Figure 4c exist here and plausible frictional variations thereof can be constructed. These solutions can arise when the value of $b$ is positive upstream, allowing branch I to be selected as the subcritical branch. Figure 7 shows two plausible examples, constructed in the manner outlined above and using the Figure 3c forcing curve ($Q = 0, \Delta < 1, \delta > 1$). The first (Figures 7a and 7b) corresponds to positive $u_2(x, w)$ while the second (Figures 7c and 7d) to negative $u_2(x, w)$. These solutions have no analogs in classical hydraulics and are distinguished by two features. First, the interface displacement (and thus the interfacial shear) are nonzero except at the virtual control. In contrast the Figure 6 solutions have zero, or very small, shear over a substantial range in $x$. Second, $d$ grows without bound as $b$ decreases and the interface can therefore detach from the side wall if $-b$ becomes large enough upstream. Ignoring the weak influence of friction, the Figure 6 solutions remain attached upstream.

[5] In nonrotating flows virtual controls occur when $|u_1| - |u_2| = 0$, which is satisfied for no shear $u_1 = u_2$ or pure exchange $u_1 = -u_2$. In our rotating case the virtual control condition is $d = 0$, which eliminates the possibility of the pure exchange condition.

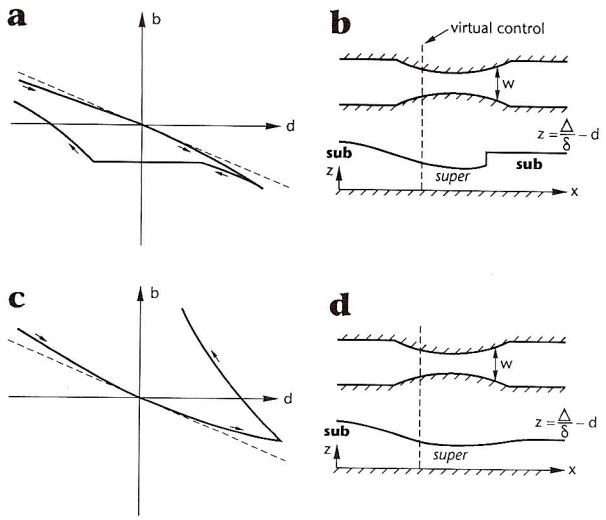


Figure 7
Same as Figure 6 but for the solution curve I-II in Figure 4c and the forcing curve of Figure 3c. Figures (a) and (b) are for positive flow in the lower layer at the wall, $u_2(x, w) > 0$ while (c) and (d) are for $u_2(x, w) < 0$.

## 8. *Discussion*

We have discussed three types of critical controls: 'narrows', 'remote' and 'virtual'. No two of these can occur separately (i.e., at different values of $x$) in the same steady flow along the same wall. However, different types of controls can occur at distinct values of $x$ at different walls. For example the left boundary layer could have a narrows control at $x = 0$, while the right boundary layer could have a virtual control at $x = -1$. The two controls would be associated with stationary Kelvin waves along the left and right walls at $x = 0$ and $x = -1$. It is not possible, however, for remote controls to occur in separate walls. (The latter would require both forcing curves to contain extrema, not a feature of the Figure 3 curves.) It is theoretically possible for remote and virtual controls to occur in pairs at different values of $x$ along a particular wall though such flows are unstable near one such point. For dual remote controls we speculate that the instability is removed through consideration of weak dispersive effects while for virtual controls the instability may be removed by friction. It is also possible for two, or all three, of the controls to occur simultaneously at the narrowest section. Finally we note that 'narrows' and 'remote' controls are dynamically linked by the fact that they occur at 'choke' points (i.e., points where the strangulation parameter $b$ reached a minimum value).

One of the most striking results of the calculation is the rich variety of critically-controlled solutions possible. It has not been possible to discuss each in detail. Is there a particular solution or group of solutions which are preferred in natural settings? Traditionally, there are several ways of attempting to answer this question. The first is to identify a 'maximal' solution in which the baroclinic mass flux is maximized over all critically-controlled solutions. One noteable application is the exchange flow in the Strait of Gibraltar, where strong mixing processes in the Mediterranean Sea are thought to produce a critically-controlled flow with maximal exchange (ARMI and FARMER, 1986). In the present asymptotic theory all solutions are independent of the baroclinic transport due to the dominance of the barotropic transport in the statement of mass conservation (3.11). Therefore, it is meaningless to seek out a 'maximal' solution without calculating higher order terms in the asymptotic expansion for wide channels.

Another means of restricting the group of acceptable solutions is to eliminate ones which have undesirable upstream characteristics. In a solution with a narrows control, for example, it is desirable to eliminate solutions which are supercritical upstream in order to avoid unstable (super-to-subcritical) transitions in the narrows. It may also be desirable to eliminate flows in which the interface is separated from either wall upstream. (For example, it may be known in advance that the baroclinic portion of the flow in the upstream basin occurs as a coastal current.) If both requirements (i.e., subcriticality and upstream attachment) are demanded, the range of potential vorticities and flow rates possible becomes restricted. In a flow with a narrows control, for example, the flow in an infinitely wide upstream basin is subcritical and attached only along branch IV of Figure 4b. This branch exists only for negative $b$ which, for large $w$, requires that $\Delta > 1$ (or $D_{10} > D_{20}$). Thus the lower layer potential vorticity must exceed that of the upper layer in order for both upstream conditions to be satisfied.

A third means of identifying 'preferred' solutions is to perform initial value experiments with simple initial states. Critically-controlled solutions are established when the initial flow is forced to adjust to a sudden decrease in the width at the narrowest section or some other abrupt change in geometry. BAINES (1984, and references contained therein) discusses similar calculations and experiments in connection with stratified, nonrotating flows. This method has the added advantage of showing *how* different solutions are established and would seem to be the next logical step in understanding the present model.

## *9. Acknowledgements*

This work was carried out under NSF Grant OCE87–00601 and ONR Contract N00014–89–K–1182. We thank Lisa Wolfe for typing the manuscript.

## *Appendix A: Calculations of Kelvin Wave Speeds*

The time-dependent version of the uniform potential vorticity, two-layer problem can be formulated by simply allowing $d$ and $\hat{d}$ to be functions of $x$ *and* $t$. The thickness and velocity profiles are thus given by (3.8) and (3.9) with $d = d(x, t)$ and $\hat{d} = \hat{d}(x, t)$. For the wave speed computation we may take the channel width as constant, $\partial w/\partial x = 0$, since nonzero $\partial w/\partial x$ merely introduces a nonhomogeneous term in the equations below.

Writing the $x$-momentum equations at the channel walls (where $v_n^* = 0$) and subtracting the lower layer result from the upper layer result gives

$$\frac{\partial}{\partial t^*}(u_1^* - u_2^*) + u_1^* \partial u_1^*/\partial x^* - u_2^* \partial u_2^*/\partial x^* + g^1 \partial D_1^*/\partial x^* = 0 \quad \text{at } y = \pm w).$$

Introducing the scaling indicated following equation (3.9) and $t = t^*F$ leads to

$$\frac{\partial}{\partial t}(u_1 - u_2) + u_1 \partial u_1/\partial x - u_2 \partial u_2/\partial x + (1 + \delta)\partial D/\partial x = 0 \quad (y = \pm w).$$

Using (3.8) and (3.9) to substitute for $u_1$ and $u_2$, evaluating the result at $y = w_1$ and taking $w \to 0$ gives

$$-(1 + \delta)d_t + u_1(-d_x) - u_2(\delta d_x) + (1 + \delta)d_x = 0$$

or

$$d_t + \lambda_+(x, t)d_x = 0 \tag{A1}$$

where

$$\lambda_+(x, t) = \frac{u_1 + \delta u_2}{1 + \delta} - 1. \tag{A2}$$

Redimensionalization of this result gives equation (5.1) for $\lambda_+$. The corresponding $y = -w$ calculation gives the $\lambda_-$ in (5.1). Note that (A2) applies to waves of arbitrary amplitude—no linear approximation has been made.

As in the case of the steady flow calculation, we have used the fact that the lowest order mass balance is barotropic. Temporal or spatial fluctuations in $d$ and $\hat{d}$ cause negligible departures of the total flow rate from its basic barotropic value. In (A1) this means that the value of $U$ (imbedded in $u_1$ and $u_2$) contains no hidden dependence upon $\partial d/\partial x$ or $\partial d/\partial t$.

## *Appendix B: Switching of Solution Branch at a Virtual Control*

In order for a solution to switch from the $d = o$ to $d = b$ branch of the solution curve in Figure 4c, it is necessary for $d_x$ to be continuous at the branch point (the

virtual control). Since $d_x = o$ for the first branch, we require $d_x = b_x w_x = o$ for the second branch. Thus the control point must also be a true control $w_x = o$, or a remote control $b_w = o$.

If we further demand that $d_{xx}$ be continuous at the virtual control, then we need

$$d_{xx} = b_{ww}(w_x)^2 + b_w w_{xx}$$
$$= 4Q(w_x)^2/[w^3(\delta - 1)] + b_w w_{xx} = o. \tag{B1}$$

At a true control ($w_x = o$, $w_{xx} > o$), it is necessary that $b_w = o$ in order to satisfy (B1). In this case, virtual, remote, and true controls all occur at the narrowest section. At a remote control ($b_w = o$, $w_x \neq o$) B1 is satisfied only if $Q = o$. The remote control condition (5.7a) then implies that $\Delta = 1$, and (4.5) in turn implies that the strangulation $b$ is constant for all $x$. The solution is thus $d = o$.

In summary, the only case where the solution can switch from one Figure 4c curve to the other is when true, virtual, and remote controls coincide ($b = b_w = d = w_x = o$). Otherwise, $d_x$ or $d_{xx}$ will be discontinuous at the control point. Inspection of Figure 3 shows that $b_w = o$ occurs only in the upper curve in upper left frame, for which $Q > 0, \Delta < 1$ (Figure 4a). The additional requirement $b = o$ implies that the minimum of this curve makes grazing contact with the $w$ axis, or

$$2(1 - \Delta)^{1/2} Q^{1/2} = 1. \tag{B2}$$

Finally, the requirement $w_x = o$ implies that the minimum $w$ occur at minimum of the same curve, or

$$w_m = Q^{1/2}/(1 - \Delta)^{1/2}. \tag{B3}$$

Combining (B2) and (B3) gives

$$w_m = 2Q.$$

## REFERENCES

ARMI, L. (1986), *The Hydraulics of Two Flowing Layers with Different Densities*, J. Fluid Mech. *163*, 27–58.

ARMI, L., and FARMER, D. M. (1986), *Maximal Two-layer Exchange through a Contraction with Barotropic Net Flow*, J. Fluid Mech. *164*, 27–51.

ARMI, L., and FARMER, D. M. (1987), *A Generalization of the Concept of Maximal Exchange in a Strait*, J. Geophys. Res. *92*(C13), 14679–14680.

ARMI, L., and FARMER, D. M. (1988), *The Flow of Atlantic Water through the Strait of Gibraltar*, Prog. Oceanogr., submitted.

BAINES, P. G. (1984), *A Unified Description of Two-layer Flow over Topography*, J. Fluid Mech. *146*, 127.

DALZIEL, S. B. (1990a), Rotating two-layer flows, in *The Physical Oceanography of Sea Straits*, NATO-ASI series (ed. PRATT, L. J.), Kluwer Inc. (to appear).

DALZIEL, S. B. (1990b), *Two-layer Hydraulics: A Functional Approach*, J. Fluid Mech., submitted.

DALZIEL, S. B. (1988), *Two-layer Hydraulics: Maximal Exchange Flows*, Ph.D. Thesis, Department of Applied Mathematics and Theoretical Physics, University of Cambridge.

FARMER, D. M., and ARMI, L. (1986), *Maximal Two-layer Exchange over a Sill and through the Combination of a Sill and Contraction with Barotropic Flow*, J. Fluid Mech. *164*, 53–76.

GILL, A. E. (1977), *The Hydraulics of Rotating-channel Flow*, J. Fluid Mech. *80*, 641–671.

HOGG, N. G. (1983), *Hydraulic Control and Flow Separation in a Multi-layered Fluid with Applications to the Vema Channel*, J. Phys. Oceanogr. *13*, 695–708.

NOF, D. (1986), *Geostrophic Shock Waves*, J. Phys. Oceanogr. *5*, 886–901.

PRATT, L. J. (1983), *On Inertial Flow over Topography. Part I. Semigeostrophic Adjustment to an Obstacle*, J. Fluid Mech. *13*, 195–218.

PRATT, L. J. (1984b), *On Nonlinear Flow with Multiple Obstructions*, J. Atmos. Sci. *41*, 1214–1225.

PRATT, L. J., and ARMI, L. (1988), *Hydraulic Control of Flow with Nonuniform Potential Vorticity*, J. Phys. Oceanogr. *17*, 2016–2029.

WHITEHEAD, J. A., LEETMAA, A., and KNOX, R. A. (1974), *Rotating Hydraulics of Strait and Sill Flows*, Geophys. Fluid Dyn. *6*, 101–125.

WOOD, I. R. (1968), *Selective Withdrawal from a Stably Stratified Fluid*, J. Fluid Mech. *32*, 209–223.

(Received November 9, 1989, accepted January 16, 1990)